Pergamon

Ocean Engng, Vol. 25, Nos 4–5, pp. 323–343, 1998
© 1997 Published by Elsevier Science Ltd. All rights reserved
Printed in Great Britain
0029-8018/98 $19.00 + 0.00

PII: S0029-8018(97)00023-1

EXPERIMENTAL INVESTIGATION OF RESPONSE STABILITY AND TRANSITION BEHAVIOUR OF A NONLINEAR OCEAN STRUCTURAL SYSTEM

Huan Lin,† Solomon C. S. Yim*† and Oded Gottlieb‡

†Ocean Engineering Program, Department of Civil Engineering, Oregon State University, Corvallis, OR 97331, U.S.A.

‡Mechanical Engineering, Technion – Israel Institute of Technology, Haifa, Israel

(*Received* 5 *December* 1996; *accepted in final form* 15 *January* 1997)

Abstract—This study experimentally investigates the nonlinear response stability and transition behaviour of a submerged, moored ocean structural system which consists of a spherical buoy and attached multi-point mooring lines. The system is excited by a periodic wave field in a closed channel. System nonlinearities include complex geometric restoring (stiffness) force and coupled fluid–system interaction exciting forces. Experimental set-up, operating procedures and analysis of the measured results are presented. Characteristic motions observed include harmonic, subharmonic and ultraharmonic responses, which demonstrate a signature of the intricate pattern of the nonlinear global behaviour. Good agreements between the measured and most predicted responses are demonstrated in both time and frequency domains. These results confirm the validity of the analytical model presented and calibrate the accuracy of the existing numerical predictions. Primary and secondary resonances in the response are identified via frequency response curves. Response bifurcation cascades are observed in the experimental results and the possible existence of higher-order nonlinear responses is inferred. © 1997 Published by Elsevier Science Ltd.

NOMENCLATURE

a	wave amplitude
A_P	projected drag area
C_A	added mass coefficient
C_D	hydrodynamic drag coefficient
C_{DL}	equivalent linear drag coefficient
C_s	effective system damping coefficient
F_D	Morison drag force
F_I	inertia force
g	gravitational acceleration
h	water depth
k	wave number
K	spring constant
l_1, l_2	lengths of mooring lines
M	mass of sphere
P_{NL}	average power of Morison drag force over N cycles
R	restoring force
$R_{(n/m,j,d)}$	resonance number
t	time

*Author to whom correspondence should be addressed.

u	fluid particle velocity
u_0	collinear current magnitude
x	surge displacement
$\dot{x}$	surge velocity
$\forall$	displaced volume
ξ_s	system damping ratio
ρ	water density
$\nu_{n(1,2)}$	peaks in the first and second half cycle in free-vibration tests
ω	wave frequency
ω_d	damped frequency in free-vibration tests

1. INTRODUCTION

Analytical and numerical models of nonlinear systems subjected to periodic excitation have revealed a variety of nonharmonic responses, instabilities and sensitivity to initial conditions (e.g. Moon, 1987). These predictions have been demonstrated through small-scale experiments where the system parameters can be accurately controlled, and the domains of attraction are easily defined and measured. Examples of these 'table-top' experiments of nonlinear aperiodic responses can be found in Moon (1987, 1992). Other examples of small-scale experimental investigations of simple single- and two-degree-of-freedom systems are reported in Popp and Stelter (1990) and Nayfeh and Balachandran (1990), respectively.

However, it may be difficult to design large-scale models to obtain chaotic responses. To the authors' knowledge to date, a large-scale fluid-structure experiment to obtain highly sensitive, nonlinear response (e.g. chaos) in the ocean has not yet been achieved. While there is an expansive amount of material on nonlinear fluid–structure interaction in the literature (e.g. Sarpakaya and Isaacson, 1981; Blevins, 1990) describing harmonic small-amplitude motions, there are only a few papers describing subharmonic responses (e.g. Lean, 1971; Thompson *et al.*, 1984; Fujino and Sagara, 1990).

A medium-scale experimental investigation of the nonlinear response of a submerged, moored, complex ocean system is reported here. The objective of this study is two-fold: (i) to experimentally determine, as much as possible, the existence of nonlinear responses (e.g. subharmonic, ultraharmonic, ultrasubharmonic, quasi-periodic and chaotic, similar to those predicted in Gottlieb and Yim, 1992), and the organized response transition in bifurcation sets predicted in the analytical study (Gottlieb *et al.*, 1997); and (ii) to assess the validity of the analytical model of a symmetric multi-point moored structural system subjected to a deterministic exciting field described by small amplitude waves and weak collinear current. The study presents a description of the submerged, moored ocean system experiment, classification of model responses and comparison of results to analytical predictions.

2. SYSTEM CONSIDERED

A general multi-degree-of-freedom, multi-point moored system is modelled by a hydrodynamically excited, submerged, rigid body moored by elastic mooring cables with geometric nonlinearity. The mooring lines considered in this study are assumed to be linear, elastic and taut, and do not vibrate transversely. These simple assumptions are in direct contrast to the nonlinear, inelastic (hysteretic), and low-tensioned cables examined by Triantafyllou and Yue (1995), where the cable properties and sag were the major sources of the nonlinear dynamical phenomena of the system response. The wave fields are gov-

erned by kinematics and return flow of prescribed periodic waves. The complex exciting force includes coupled fluid–structure interaction drag and inertial terms. The drag/lift is quadratic in nature whereas the inertial components consist of a linear O(1) temporal term and O(ϵ) nonlinear convective terms which become increasingly important near system resonances (Gottlieb and Yim, 1992).

2.1. *Model configuration*

The general experimental configuration is formulated with an intention of calibrating the various nonlinear response behaviours predicted by corresponding analytical models, including the existence of subharmonics, ultraharmonics and the organized response transition (Gottlieb *et al.*, 1997).

The experimental models considered in this study are geometrically nonlinear two- and four-point moored single-degree-of-freedom (SDOF) systems in surge. The models consist of a sphere on a rod supported by guyed masts six feet above the bottom of a closed wave channel (Fig. 1). Spheres made of PVC with diameters of 11 and 18 in were used. Two Delrin bearings were placed on the spheres to reduce the friction and minimize the free-

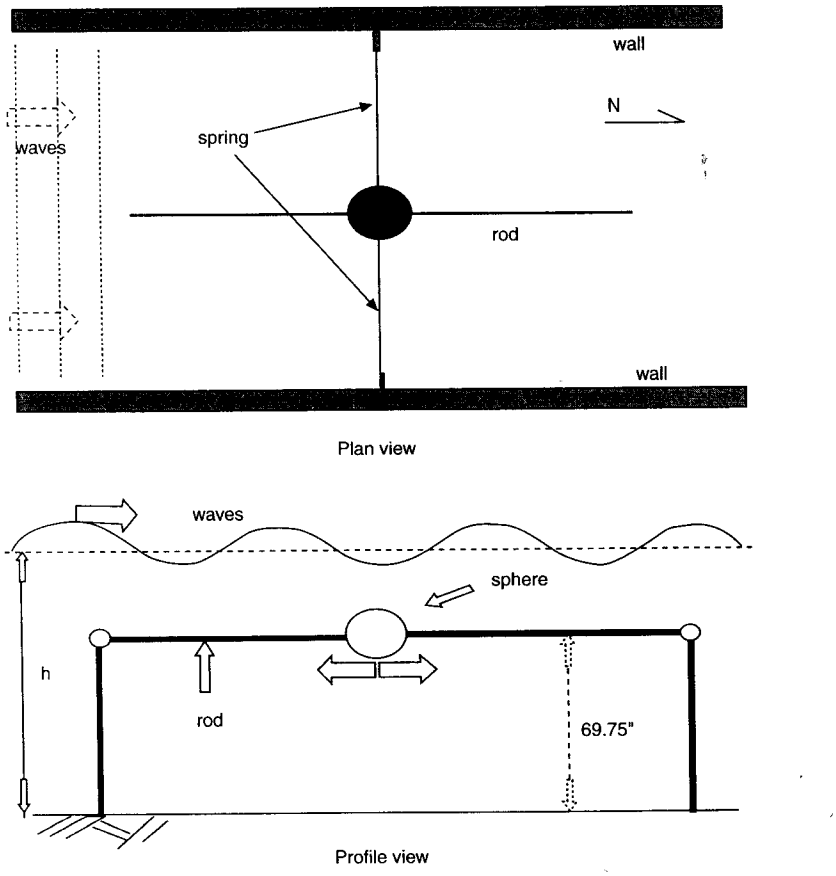

Fig. 1. SDOF experimental model (90° configuration).

play between the sphere and the rod. The spheres were filled with water when submerged. The in-air weight of the 11 in sphere was 7 lbs empty and 25 lbs when filled with water. The 18 in sphere weighed 25 lbs empty and 106 lbs filled. Springs of various stiffness (10 or 20 lbs/ft) were attached to the sphere at an angle of 60 or 90° to provide a nonlinear restoring force (Fig. 2). The restoring force, which contains geometric nonlinearity, can be derived by a Lagrangian formulation (Gottlieb and Yim, 1992). The damping mechanism includes a linear system (structural) component (associated with the system connections and contact points of instrumentation), and a time-dependent coulomb friction component (due to the set-up of restricted surge motion). The coulomb friction originates from the lift force (in heave) and combined drag/lift moment (in pitch). The variability in the friction force is a result of changing amplitude and direction of normal force due to the oscillatory nature of the hydrodynamic drag/lift forces.

The initial tension in the mooring cables was varied from 15 to 30 lbs depending on the test case. The majority of the tests were performed with relatively low initial tension (25 lbs) to ensure nonlinear motion response (Gottlieb and Yim, 1992).

2.2. *Equation of motion*

Assuming the time-dependent effects of the coulomb friction can be lumped into an equivalent linear system damping coefficient, the equation of motion of the cable moored system is given by

$$M\ddot{x} + C_s\dot{x} + R(x) = F_D(x,\dot{x}) + F_I(\dot{x},\ddot{x}) \tag{1}$$

where x and $\dot{x}$ denote the surge displacement and velocity, respectively; M the mass of the system; R the nonlinear restoring force; C_s the effective system damping coefficient; F_D and F_I the drag and inertial components of the exciting force, respectively.

The restoring force includes the force due to the mooring (R_M) and the force due to hydrostatic buoyancy (R_B). The spheres used for this experiment were virtually neutrally

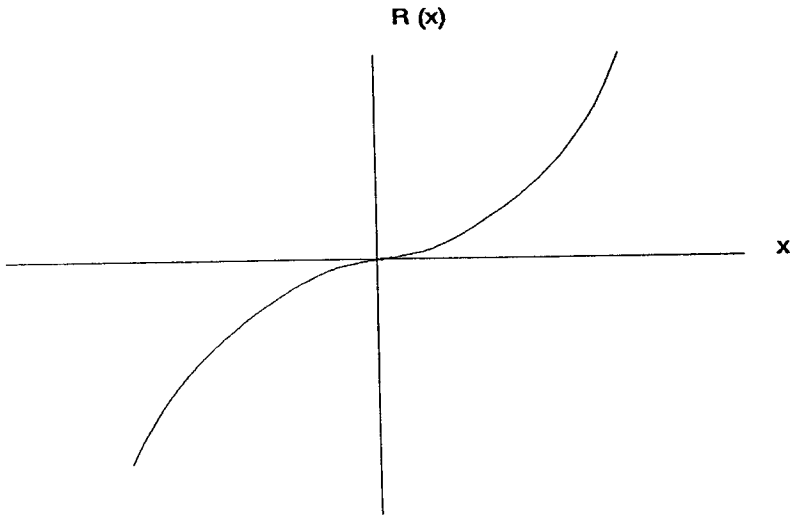

Fig. 2. Restoring force diagram.

buoyant when submerged. Therefore, the forcing caused by R_B was negligible and is not considered here. The restoring force $R(x)$ is then given by

$$R(x) \cong R_M = K\left[4x + l_c\left(2b\,\frac{l_1 - l_2}{l_1 l_2} - 2x\,\frac{l_1 + l_2}{l_1 l_2}\right)\right] \tag{2}$$

where K is the spring constant and b governs the spring configuration ($b = 0$ for 90° and $b = l_{1,2}/2$ for 60°, respectively). $l_{1,2}$ are the spring lengths and l_c is the initial spring length. The exciting force consists of a relative Morison drag (F_D) and an inertial component (F_I):

$$F_D = \frac{\rho}{2} C_D A_P (u - x)|u - \dot{x}| \tag{3a}$$

$$F_I = \rho\forall(1 + C_A)\left[\frac{\partial u}{\partial t} + (u - \dot{x})\,\frac{\partial u}{\partial x}\right] - \rho\forall C_A\ddot{x} \tag{3b}$$

with

$$u = u_0 + \omega a\,\frac{\cosh(kh)}{\sinh(kh)}\cos(kx - \omega t) \tag{3c}$$

where C_D is the hydrodynamic viscous drag coefficient; C_A the added mass coefficient; A_p the projected drag area; $\forall$ the displaced volume. u_0 represents the collinear current magnitude; a the wave amplitude; ω the wave frequency; k the wave number; ρ the water density; g the gravitational acceleration; and h the water depth.

3. ANALYTICAL PREDICTIONS

For convenience of reference and comparison with experimental results in later sections, analysis and numerical predictions by Gottlieb *et al.* (1997) are briefly summarized here.

Using the method of harmonic balance, approximate solutions to Equation (1) can be obtained. Local stability analyses on the approximate solutions are conducted using Hill's variational technique, and the primary and secondary resonances can be identified in the parameter space. In addition to the analytically identified lower-order resonances, the higher-order are also observed via extensive numerical simulations. With the analytical and numerical results, a universal pattern underlying the bifurcation set is found to exist (Fig. 3).

To classify the bifurcation pattern of the nonlinear responses (e.g. subharmonic, ultraharmonic, and ultrasubharmonic), a resonance number $R_{(n/mj,d)}$ is employed. Using the nonlinear resonance relationship $n\omega \approx m\sqrt{\alpha_1}$ (where ω is the wave excitation frequency; α_1 the coefficient of the linear component of the nonlinear stiffness), the first index $[n/m]$ of the resonance number is employed to classify the characteristic periodic responses. The second index $[j]$ is used to determine the order of ratios with noncommon factors. Finally, the third index is used to describe the dimension $[d]$ of the response (i.e. integer deterministic versus fractal chaotic).

A bifurcation pattern diagram of system responses can be constructed (Fig. 4) via numerical simulations and the classification criterion summarized above. The diagram depicts the existence of periodic orbits throughout the domain described by a variety of subharmonic and ultraharmonic solutions. Solutions are separated by a common periodicity

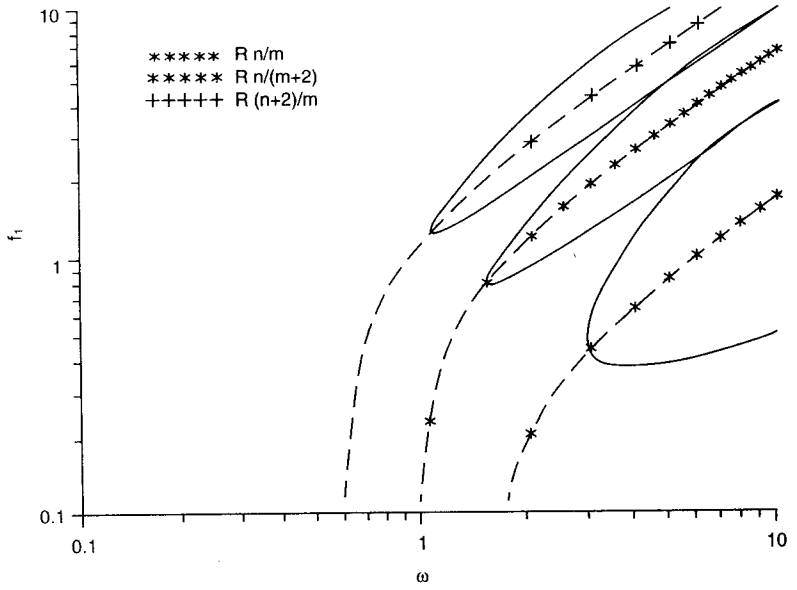

Fig. 3. Superstructure in bifurcation sets.

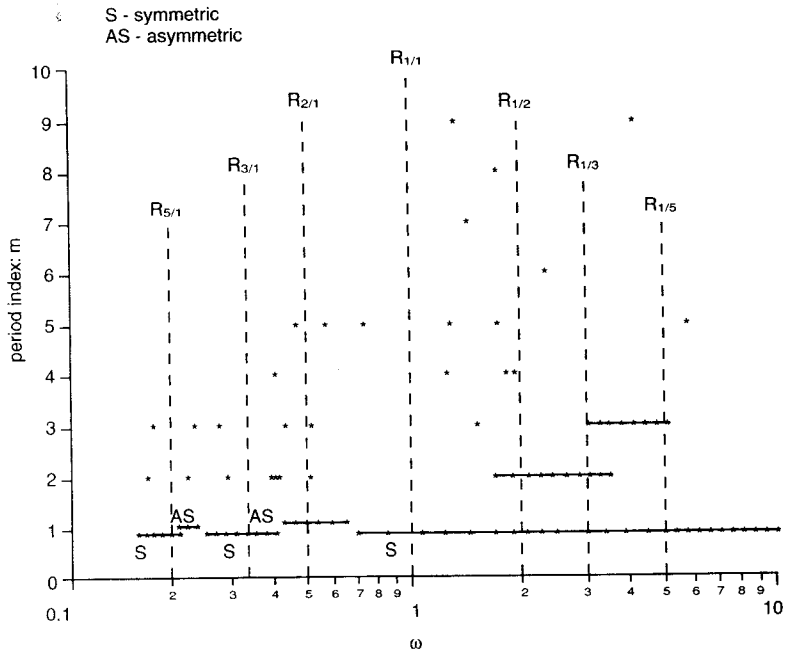

Fig. 4. Bifurcation diagram.

index m. Symmetric (S) and asymmetric (AS) solutions describing pitchfork bifurcation transition are also depicted. Resonance lines ($R_{n/m}$: dashed lines) are added to highlight solution ordering. This diagram will be used as a guideline for experimental search of higher-order nonlinear responses as well as a baseline for comparison.

4. EXPERIMENT DESCRIPTION

The experiment was conducted at the O. H. Hinsdale Wave Laboratory at Oregon State University in a two-dimensional wave channel, which is 342 ft long, 12 ft wide and 15 ft deep with a hydraulically driven, hinged flap wave board (Fig. 5). A VAX 3400 server and two VAX 3100 stations with optical communication links for wave generation control and 64 digital channels were used for data acquisition.

The model tests were divided into four distinct phases. The first phase was with a small sphere moored at 90° angles; the second with the small sphere at 60°; the third with a large sphere at 60°; and the last with the large sphere at 90° (Yim *et al.*, 1993).

Data recorded during each test included wave profiles at several locations along the channel, currents, sphere displacements, and tensions in the springs. The wave profiles were measured by six resistive type wave gauges. MINILAB, model SD-12, current meters were used to measure the horizontal and vertical velocities of the water particles. UniMeasure, model P-75A, string pots were used to measure the displacements of the spheres. Strain gauges were placed on the lines connecting the springs to the spheres to measure the components of the restoring force. The initial (static) value of the spring tension could be adjusted by tightening/loosening the springs from the carriage above. Two underwater cameras were used to provide a second means of measuring the spheres' displacements. The cameras also provided visualization of the displacements of the spheres.

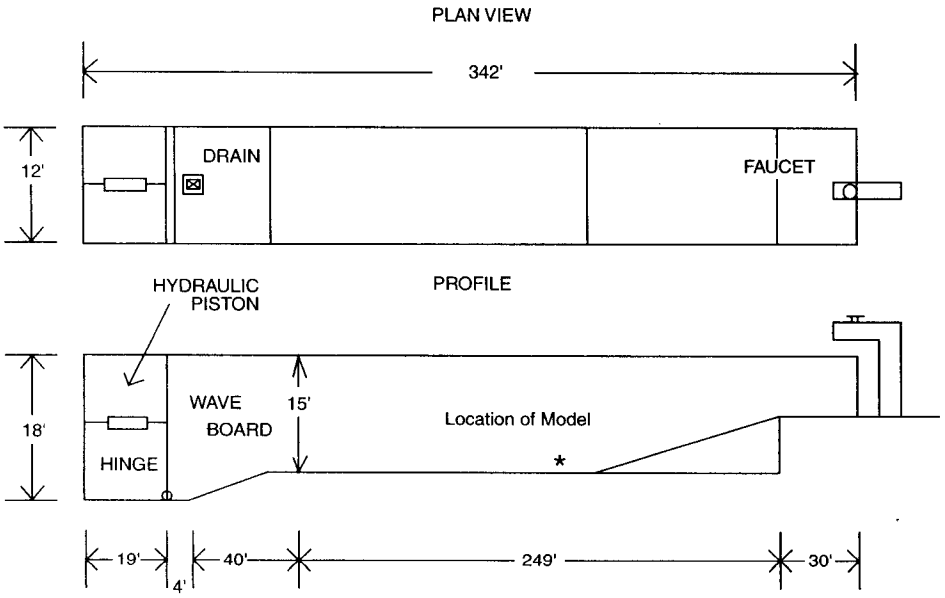

Fig. 5. Two-dimensional wave flume.

Three wave gauges were placed on each side of the model at distances of 1.5, 4.0 and 11.0 ft from the model. The current meter was placed 10 in upstream of the model, 22 in from the side wall at a depth of 9 in. Two string pots were attached to the sphere for displacement measurements on opposite sides to offset the force placed on the sphere by the string pots. Two string pots on the 90° configuration and four string pots on the 60° configuration were used to measure the elongation of the springs which were used to determine the restoring forces.

Data describing the wave profile, current and sphere displacement were collected, conditioned, filtered, and stored on a VAX 3400. 14 data channels were used to collect information from the measurement instruments.

5. TEST TYPES

5.1. *Free-Vibration tests*

Free-vibration tests were first conducted to gain an understanding of the hydrodynamic effects on system damping to provide an initial estimate of the damping coefficients. A total of 31 tests were conducted in still water.

These tests were performed on both the large and small spheres at the 60° and 90° configurations by manually displacing and then releasing the sphere and measuring the response. In addition to hydrodynamic damping, coulomb damping due to configuration constraints is another source of energy dissipation. However, because the model was neutrally buoyant in water, the normal force between the sphere and the supporting rod was negligible. Hence frictional force was significantly smaller. Damping in this case is caused mostly by hydrodynamics.

5.2. *Continuous search tests*

The stability of the response of the nonlinear moored system subjected to periodic excitation can be predicted by referencing the backbone curve of the corresponding analytical model (Gottlieb and Yim, 1992). To identify changes in response stability, the systems were subjected to waves with approximately constant amplitudes but with gradually varying frequencies. Due to the fixed dimensions of the wave channel, wave mechanics relationships and limitations in wave generating capacity, it was not always possible to keep the wave height constant as the frequency was varied. Despite variations in the wave height causing difficulties in interpreting the experimental results, stability changes in response were clearly observed.

There were four search test runs performed on the large sphere with the 60° and 90° configurations. In the continuous search mode, the wave frequencies were normally changed by 0.01 Hz every 2–3 min. Excitation parameters (frequencies and amplitudes) were manually recorded and would be used in data acquisition tests to further examine the interesting nonlinear phenomena observed.

5.3. *Data acquisition tests*

Four sets of data acquisition tests were performed to obtain steady-state responses. The tests examined can be categorized based on the size of the sphere and the configuration as: the small sphere with 90° configuration, small sphere with 60°, large sphere with 60°, and large sphere with 90°.

Data acquisition tests were initially performed at frequencies and wave heights at which nonlinear responses of specific characteristics may be expected based on the existing analytical study (Gottlieb *et al.*, 1997). The small sphere was used in the first two sets of tests. However, it was observed that for a significant number of the cases tested, the response amplitudes were not sufficiently large to reach the nonlinear regime. The smaller (11 in) sphere was thus replaced with the larger (18 in) sphere to obtain larger hydrodynamic forcing and nonlinear system responses. Data acquisition tests were then performed near frequencies and wave heights at which nonlinear behaviour was observed in the continuous search tests. The lengths of the tests varied from 5 to 30 min to assure steady-state behaviours. Because the initial conditions of the search tests were not precisely known, several tests around these regions with various initial conditions were performed to identify coexisting nonlinear responses.

6. ANALYSIS OF EXPERIMENTAL RESULTS

6.1. *Free-Vibration tests*

The energy dissipation mechanism of the model includes system (structural) and hydrodynamic damping components. Assuming the system damping remains the same in still water and under waves, an approximate system damping force can be separated from the hydrodynamic component based on the data from the free-vibration tests. The equation of motion of the sphere in still water is obtained by setting the fluid particle velocity u to zero in Equation (3a):

$$M\ddot{x} + C_s\dot{x} + R(x) = \frac{\rho C_D A_P}{2}(-\dot{x})|\dot{x}| - \rho\forall C_A\ddot{x} \tag{4}$$

Response amplitudes in the free-vibration tests were observed as exponentially decreasing, and the response velocity of the nth cycle can be assumed as

$$\dot{x}_n(t) = \nu_{n(1,2)}\cos(\omega_d t + \phi) = \nu_{n(1,2)}\cos(\theta),\quad \theta = \omega_d t + \phi \tag{5}$$

where $\nu_{n(1,2)}$ are the peaks in the first and second half cycles, respectively, and ω_d is the damped frequency. Equating the amount of energy dissipated over the entire data record of a test, the total nonlinear damping force can be represented in an equivalent linear form to isolate the system (structural) damping.

The average power due to nonlinear Morison drag force over N cycles is given by

$$P_{NL} = \frac{1}{2N\pi}\left[\int_0^{\pi}\dot{x}_1(\theta)\,\frac{\rho C_D A_P}{2}\,\dot{x}_1(\theta)|\dot{x}_1(\theta)|\,d\theta + \int_{\pi}^{2\pi}\dot{x}_1(\theta)\,\frac{\rho C_D A_P}{2}\,\dot{x}_1(\theta)|\dot{x}_1(\theta)|\,d\theta \ldots + \int_{(2N-2)\pi}^{(2N-1)\pi}\dot{x}_N(\theta)\,\frac{\rho C_D A_P}{2}\,\dot{x}_N(\theta)|\dot{x}_N(\theta)|\,d\theta + \int_{(2N-1)\pi}^{2N\pi}\dot{x}_N(\theta)\,\frac{\rho C_D A_P}{2}\,\dot{x}_N(\theta)|\dot{x}_N(\theta)|\,d\theta\right] = \frac{\rho C_D A_P}{3N\pi}(\nu^3_{1(1)} + \nu^3_{1(2)} \ldots + \nu^3_{N(1)} + \nu^3_{N(2)}) \tag{6}$$

where N represents the maximum number of complete cycles in a free-vibration test. The average power due to a linear drag force over N cycles is

$$P_L = \frac{1}{2N\pi}\left[\int_0^{\pi} \dot{x}_1(\theta)\ \frac{\rho C_{DL} A_P}{2}\dot{x}_1(\theta)\,d\theta + \int_{\pi}^{2\pi} \dot{x}_1(\theta)\ \frac{\rho C_{DL} A_P}{2}\dot{x}_1(\theta)\,d\theta \ldots\right.$$
$$\left. + \int_{(2N-2)\pi}^{(2N-1)\pi} \dot{x}_N(\theta)\ \frac{\rho C_{DL} A_P}{2}\dot{x}_N(\theta)\,d\theta + \int_{(2N-1)\pi}^{2N\pi} \dot{x}_N(\theta)\ \frac{\rho C_{DL} A_P}{2}\dot{x}_N(\theta)\,d\theta\right] \tag{7}$$
$$= \frac{\rho C_{DL} A_P}{8N}\left(v_{1(1)}^2 + v_{1(2)}^2 \ldots + v_{N(1)}^2 + v_{N(2)}^2\right)$$

where C_{DL} represents the equivalent linear drag coefficient.

Defining r as an average rate of velocity amplitude decrement ($v_{1(2)} = rv_{1(1)}, \ldots, v_{N(2)} = rv_{N(1)}$) and equating Equations (6) and (7), the equivalent linear drag coefficient C_{DL} is thus given by

$$C_{DL} = \frac{8C_D}{3\pi}\hat{r}v_1 \tag{8a}$$

with

$$\hat{r} = \frac{1 + r^3}{1 + r^2};\ r \cong \frac{1}{N}\left(\frac{v_{1(2)}}{v_{1(1)}} + \frac{v_{2(2)}}{v_{2(1)}} \ldots + \frac{v_{N(2)}}{v_{N(1)}}\right) \tag{8b}$$

Assuming the motions are not too large, the restoring force $R(x)$ can be equivalently linearized and approximated by $k_1 x$. By rearranging, an equivalent linear version of Equation (4) can be simplified and rewritten as

$$M\ddot{x} + C_{eq}\dot{x} + k_1 x = 0 \tag{9a}$$

with

$$\tilde{M} = M + \rho C_A \forall;\ C_{eq} = C_s + \frac{4\rho C_D v_1 A_P \hat{r}}{3\pi} \tag{9b}$$

For linear systems (e.g. Equation (9a)), damping coefficients can be represented by

$$C_{eq} = \xi C_{cr} \tag{10a}$$

with

$$\xi = \frac{\delta}{\sqrt{4\pi^2 + \delta^2}};\ \delta = \frac{1}{N-1}\ln\frac{a_1}{a_N};\ C_{cr} = 2\tilde{M}\omega_0;\ \omega_0^2 = \frac{k_1}{\tilde{M}} \tag{10b}$$

where a_1 and a_N are the positive peaks in the first and Nth cycles, respectively. C_{cr} denotes the critical damping; ξ the damping ratio; and ω_0 the natural frequency.

Applying Equations (8b) and (9b), the system damping ratio ξ_s can be computed as

$$\xi_s = \frac{C_s}{C_{cr}} \; ; \; C_s = C_{eq} - \frac{4\rho C_A \nu_1 A_P \hat{r}}{3\pi} \tag{11}$$

Fig. 6 shows a typical free-vibration test compared with the exponential decrement based on the equivalent linearization procedure described above. This specific test was conducted on the small sphere with the 90° configuration and 25 lbs initial tension in springs. The system damping ratio is determined to be 7.0%. Close fitting of the exponential curves to the peaks of the test indicates that the effects of the quadratic drag can be effectively modelled by an equivalent linear damping. Note that the effects due to time-varying, excitation-dependent coulomb damping are lumped in the system damping, hence the actual system damping coefficients in data acquisition tests vary from case to case. Nevertheless, the estimated system damping coefficients provide an initial estimate for further system parameter identification described in a later section.

6.2. *Continuous search tests*

The first and second search tests were performed on the large sphere with the 60° configuration. In the first search test, the wave height was kept constant at 0.90 ft and the frequency was increased from 0.41 to 0.70 Hz with an increment of 0.01 Hz. The response amplitude steadily decreased as the frequency increased.

In the second search test, the frequency was decreased from 0.70 to 0.13 Hz with a decrement of 0.01 Hz. The wave height increased from 1.2 to 2.09 ft in going from 0.70 to 0.45 Hz and the response amplitude increased as the wave height increased and frequency decreased. The search tests were designed to identify specific nonlinear phenomena, which

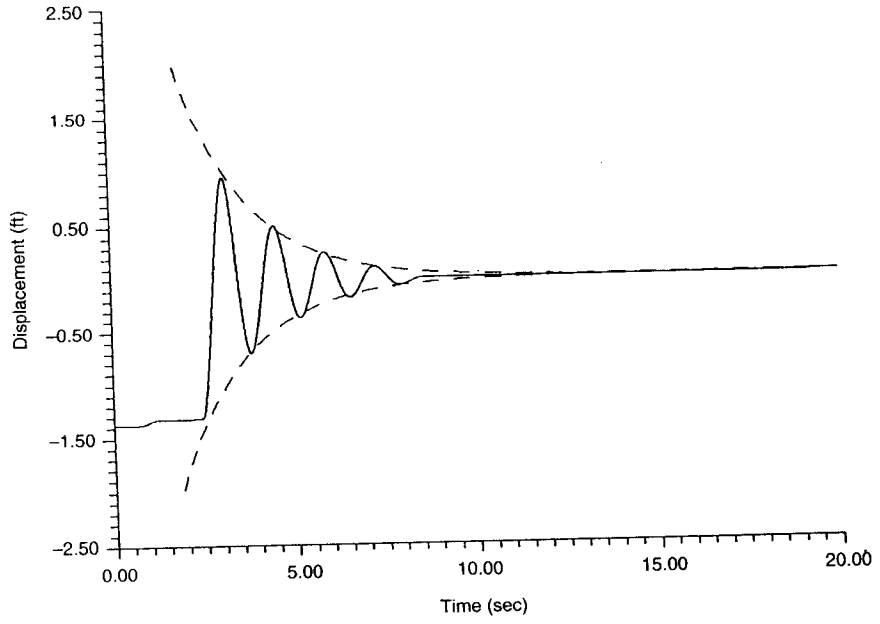

Fig. 6. Free-vibration (test P8F, small sphere with 90° configuration and 20 lbs initial tension); measured data (solid line) and exponential decrement (dashed line) based on linear approximation.

could be more frequently observed in large amplitude responses. However, to prevent the response from becoming too large and damaging the test model, the maximum response amplitude was maintained at about 36 in by adjusting the wave height as necessary when the frequency was varied.

The third and fourth search tests were performed on the large sphere with the 90° configuration. For this geometric configuration, nonlinear behaviour can be achieved at a much lower amplitude. In the third search test, the excitation frequency first increased from 0.10 to 1.00 Hz and then decreased from 1.00 to 0.10 Hz. During this test ultraharmonic responses were observed from 0.15 to 0.18 Hz and period doubling was observed from 0.46 to 0.56 Hz. Ultraharmonic responses were also observed from 0.14 to 0.12 Hz and a possible transition point from ultraharmonic to subharmonic response was observed at 0.11 Hz.

The fourth search test was intended to further investigate the nonlinear phenomena observed previously. For instance, the transition near 0.11 Hz from ultraharmonic to subharmonic observed in the third search test was examined here to pinpoint the bifurcation point. However, steady-state responses observed were strictly ultraharmonic with no identifiable transition region. The disappearance of the transition may be due to the response sensitivity to initial conditions and excitation variations.

Figs 7a and 7b show the characteristic frequency response with the 60° and 90° configurations, respectively. As noted previously, to maintain the sphere response sufficiently large for nonlinear behaviour without damaging the model, wave amplitude and frequency need to accordingly be manoeuvred at the same time. A nonlinear relationship between response and excitation in a three-parameter space can be interpreted by plotting amplitude ratio (response amplitude/wave amplitude) against excitation frequency instead of a standard frequency response curve (Nayfeh and Mook, 1979). Resonances and nonlinear relationships between the system response and the excitation are fully revealed in Fig. 7.

It is shown that for the 60° configuration the primary resonance, $R_{1/1,1}$ (cf. Figs 3 and 4), is located near 0.4 Hz and the backbone curve tilts over to the right due to its hardening stiffness. A secondary resonance, $R_{2/1,1}$ (cf. Fig. 3), is also shown near 0.2 Hz, thus loss of response stability may be observed near the region. Based on the experimental search test observations, harmonic responses become unstable and transition to ultraharmonic occurs within the frequency range 0.17–0.25 Hz (cf. Fig. 4).

The relationship of sphere response and wave with the 90° configuration is shown in Fig. 7b. The primary resonance is located near 0.27 Hz ($R_{1/1,1}$), and two secondary resonances are observed near 0.14 Hz ($R_{2/1,1}$) and 0.53 Hz ($R_{1/2,1}$), respectively (cf. Fig. 5). Note that, despite the fact that the primary resonance tilts over to the right, the low frequency secondary resonance (0.14 Hz) leans over to the left, which agrees with the numerical result of Parlitz and Lauterborn (1985). Transitions between harmonic and ultraharmonic responses were observed in the experiment near 0.11 and 0.16 Hz, and ultraharmonic response dominates the system behaviour within the wave frequency range 0.11–0.16 Hz. The loss of response stability near resonance regions is analytically predicted (Gottlieb *et al.*, 1997). Period doublings were also observed in the experiment near the location of high frequency secondary resonance (0.53 Hz). Within the frequency range 0.46–0.56 Hz, period doubling bifurcations were frequently observed, and a signature of bifurcation superstructure is indicated to exist in the moored system (cf. Fig. 4).

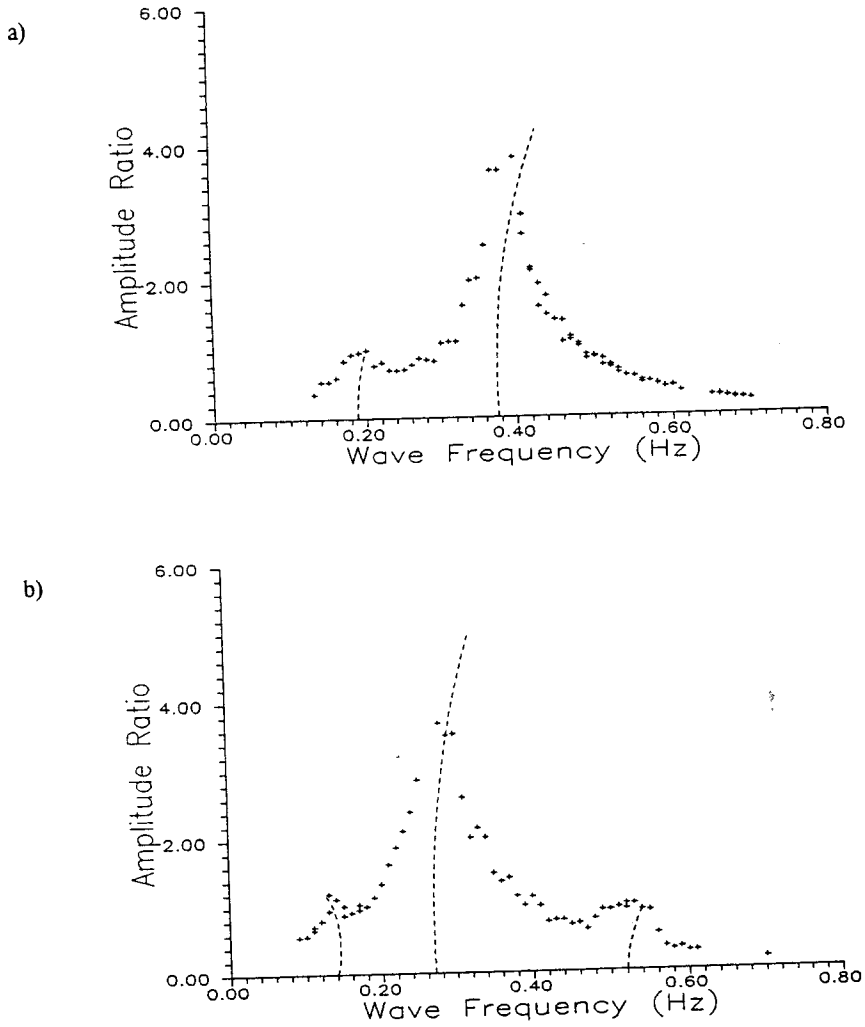

Fig. 7. Frequency response ratio (response amplitude/wave amplitude) versus wave frequency: (a) large sphere with 60° configuration; (b) large sphere with 90° configuration.

6.3. *Response to periodic excitation*

6.3.1. *Experimental observations*. To demonstrate the variety and complexity of the system responses, examples of typical responses are presented in this section (see Yim *et al.*, 1993 for a detailed description and preliminary analysis of measured data).

In addition to the few ultraharmonic responses observed, the response of the small sphere with the 90° and 60° configurations mostly behaved in a harmonic fashion (e.g. see Fig. 8). Some ultraharmonic responses for the large sphere with the 60° configuration were observed (e.g. Fig. 9). These ultraharmonic responses appeared strongly stable, reaching steady-state within a few cycles of the excitation and remaining throughout the test.

Because of its strong complex geometric nonlinearity, the large sphere with the 90°

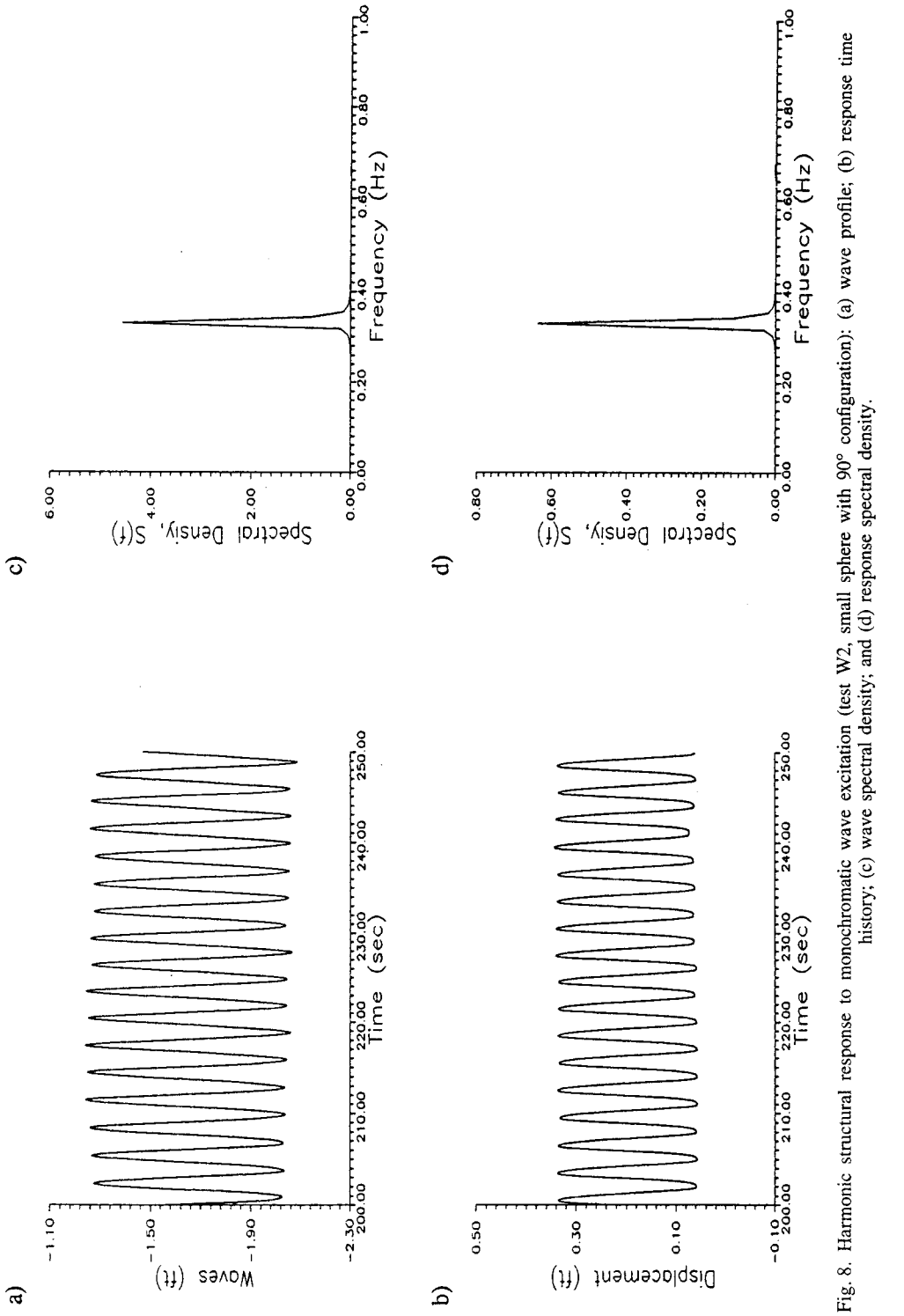

Fig. 8. Harmonic structural response to monochromatic wave excitation (test W2, small sphere with 90° configuration): (a) wave profile; (b) response time history; (c) wave spectral density; and (d) response spectral density.

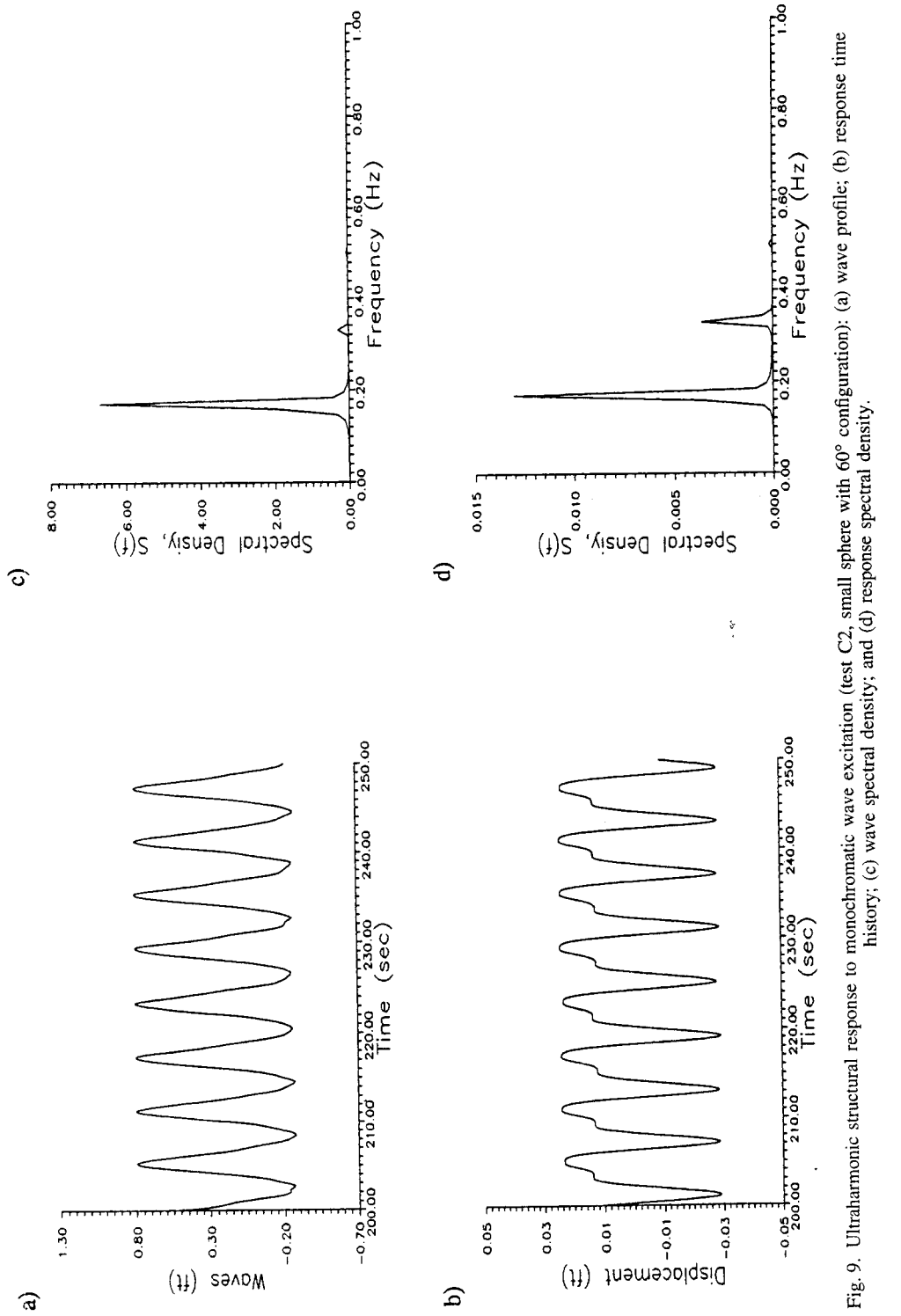

Fig. 9. Ultraharmonic structural response to monochromatic wave excitation (test C2, small sphere with 60° configuration): (a) wave profile; (b) response time history; (c) wave spectral density; and (d) response spectral density.

configuration exhibited the most interesting nonlinear responses as predicted. Both subharmonic (e.g. Fig. 10) and ultraharmonic responses (e.g. Fig. 11) were frequently observed.

6.3.2. *Comparisons and discussions.* The validity of the analytical model (Equation (1)) can be examined by comparing simulated solutions with experimental results. Parameters of the analytical model are identified for a combination of configurations using simulated results based on the free-vibration tests and a reverse multiple-input–single-output (R-MISO) technique (Bendat and Piersol, 1993).

Stiffness coefficients are calculated based on a least-square approximation of the mooring spring configurations. The analysis of the free-vibration tests in the previous section provides an estimate for the system damping coefficient. The reverse MISO technique identifies the system natural frequency and estimates the drag and added mass coefficients by treating nonlinear terms as inputs and inverting the standard linear analysis procedure. The system damping, drag and added mass coefficients are later fine-tuned via numerical simulations.

Experimental responses are compared to corresponding simulated solutions (using the estimated parameters) via time series (Figs 10b and 11b) and energy spectra (Figs 10d and 11d). For both ultraharmonic (Fig. 10) and subharmonic (Fig. 11) responses, the numerical predicted motions provide good agreement in both response amplitude and phase shift in time domain. Compared to the measured data, deviations in the energy spectra of the simulations in both cases are within 10%.

It is well-known that the added mass coefficients and drag coefficients are wave frequency-dependent, which cannot be fully described by the Morison hydrodynamic force. Therefore, the parameters used for the analytical model need to be identified on a case-by-case basis. However, the results shown here indicate that the Morison force representation can capture the hydrodynamic behaviour within the range considered. With sufficiently large size of data collected and parameters identified accordingly, the analytical model can be expected to provide reasonably accurate predictions.

The existence of harmonic, subharmonic and ultraharmonic responses in the experimental model clearly demonstrates the highly nonlinear nature of the moored system responses. However, due to physical limitations of the experimental model and laboratory facilities, the relatively small number of tests conducted, and the restrictive quiescent initial condition for all tests, no obvious deterministic higher-order nonlinear steady-state nonlinear responses (e.g. quasi-periodic and chaotic) were identified. In spite of these limitations, the experimental observations (especially Fig. 7) along with the analytical/numerical predictions illustrated in Fig. 7 indicate that high-order nonlinear responses may reside in the transient portion or in the domain of attraction other than quiescent initial conditions.

Besides the steady-state nonlinear responses, transitions from one response state to another, which cannot be explained by deterministic analysis, were observed in the experiment (Fig. 12). Initially, the system response behaved in a harmonic fashion for about 120 s (Fig. 12a) and then transitioned (Fig. 12b) to a subharmonic steady-state (Fig. 12c). This transition may be induced by the presence of uncontrollable noise which is caused by a combination of reflection, re-reflection, wave diffraction by the model, and imperfect energy dissipation at the beach of the testing facilities. A stochastic analysis approach taking into account this uncontrollable noise may be needed to further investigate the observed nonlinear responses.

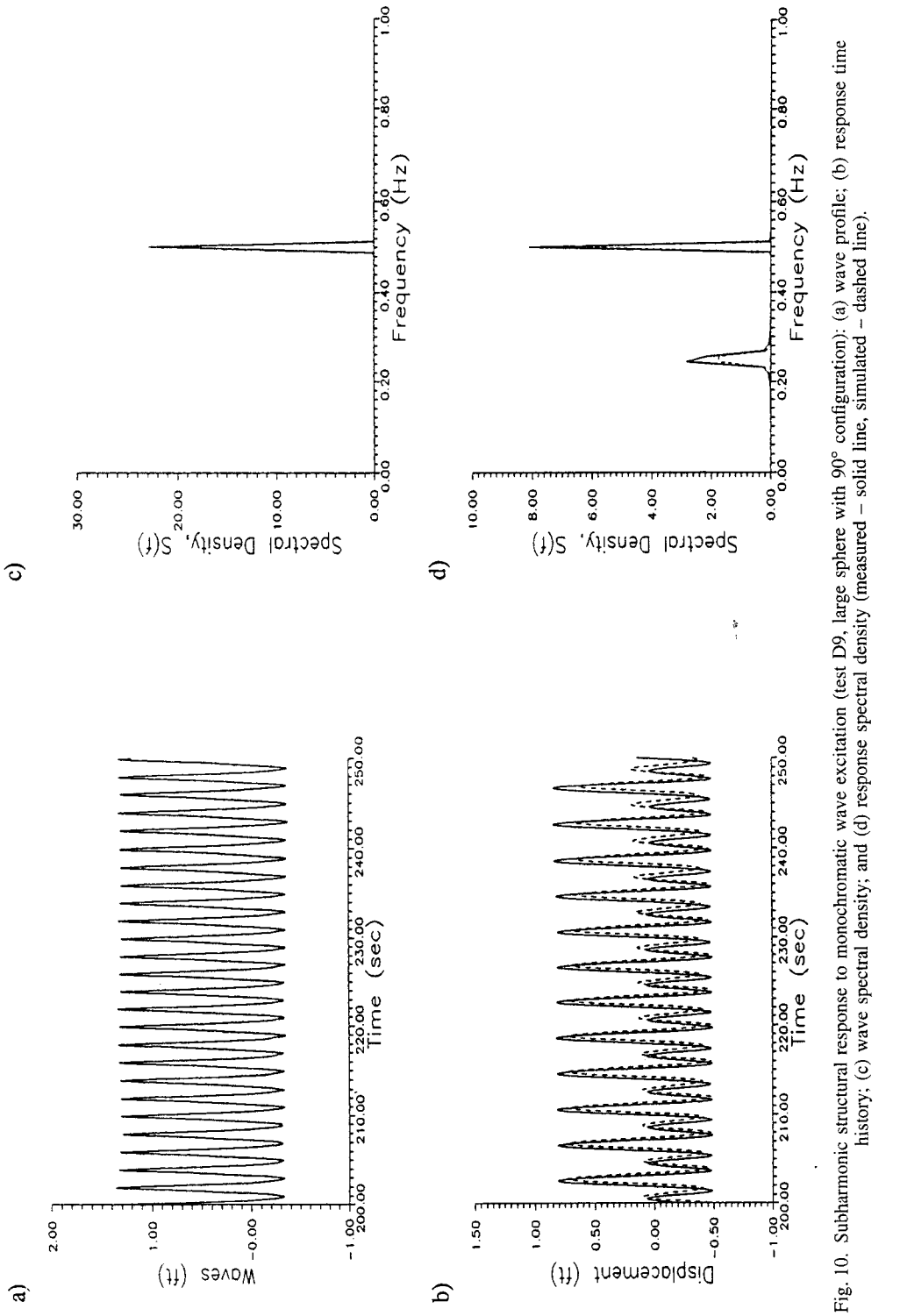

Fig. 10. Subharmonic structural response to monochromatic wave excitation (test D9, large sphere with 90° configuration): (a) wave profile; (b) response time history; (c) wave spectral density; and (d) response spectral density (measured – solid line, simulated – dashed line).

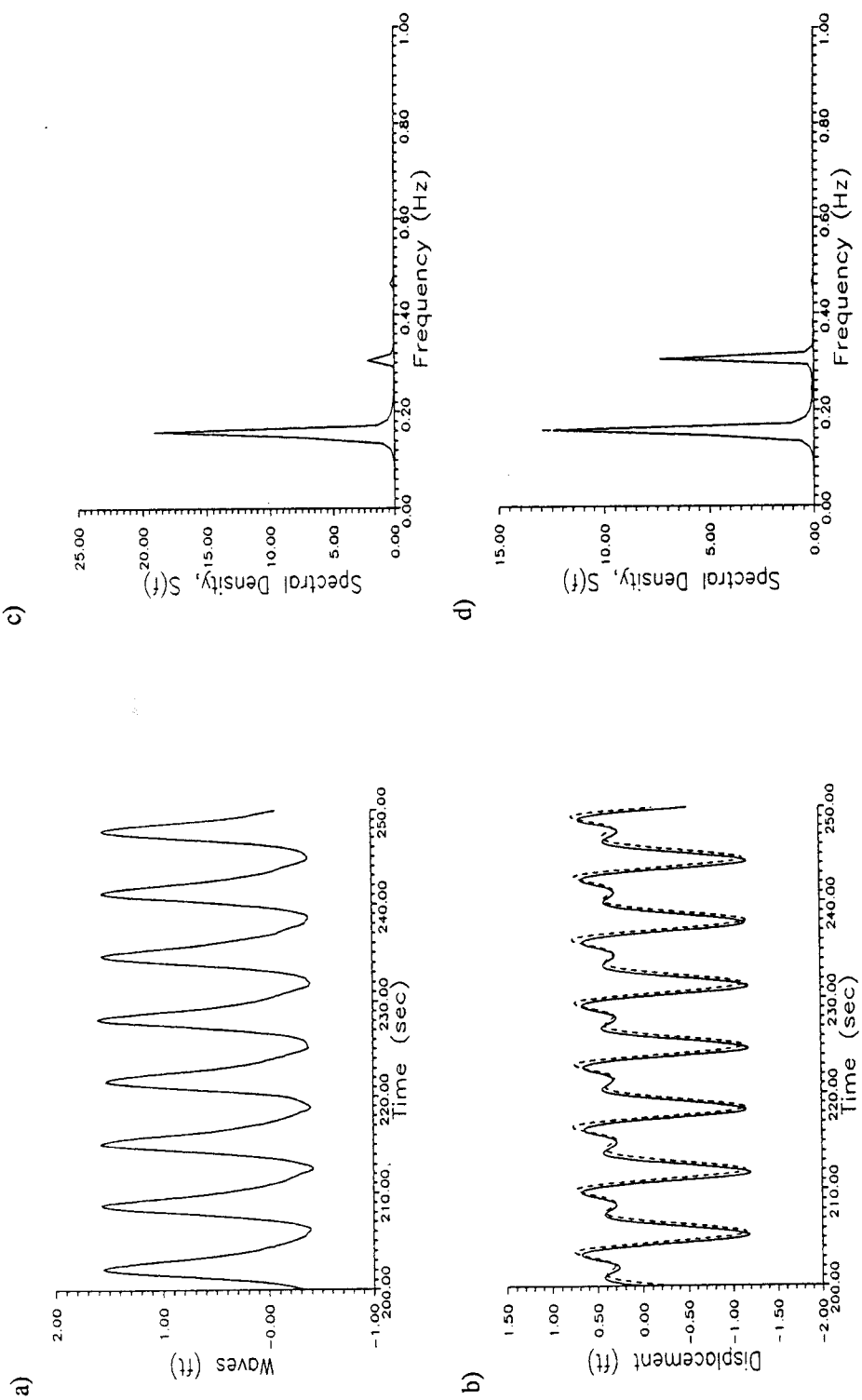

Fig. 11. Ultraharmonic structural response to monochromatic wave excitation (test D3, large sphere with 90° configuration): (a) wave profile; (b) response time history; (c) wave spectral density; and (d) response spectral density (measured – solid line, simulated – dashed line).

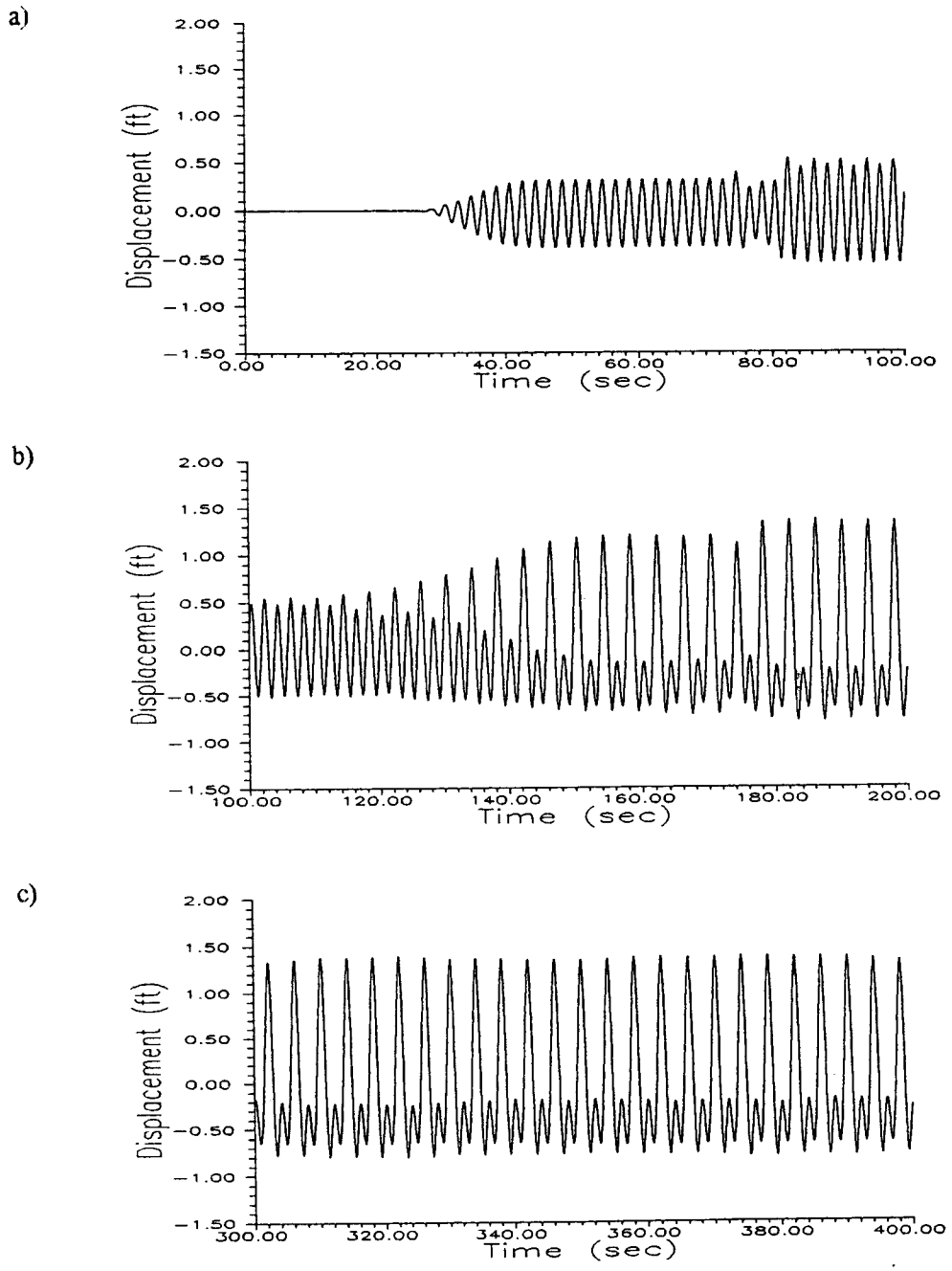

Fig. 12. Transition from harmonic to subharmonic in response behaviour (test D2, large sphere with 90° configuration): (a) transient harmonic; (b) transition from harmonic to subharmonic; and (c) steady-state subharmonic response.

7. CONCLUDING REMARKS

An experimental investigation of the stability of nonlinear response stability and the transition behaviour of a moored ocean structural system is presented here. Configurations of the experimental model and parameters of the wave excitation are designed based on the existing analytical model and predictions.

Nonlinear experimental responses, including harmonic resonance, subharmonic and ultraharmonic, have been observed. These results corroborate the complex nonlinear system behaviour predicted by those of the analytical model. Frequency response curves demonstrate a nonlinear relationship between the wave excitation and system responses in parameter space. Primary ($R_{1/1,1}$) and secondary ($R_{2/1,1}$, $R_{1/2,1}$) resonances are exhibited in the curve, and the possible existence of a bifurcation superstructure and route to chaotic response is implied. Good agreement between numerical simulations and experimental responses is shown, and the validity of the analytical model is demonstrated. Due to limitations in precision control of the wave field and system parameters, no obvious deterministic higher-order steady-state nonlinear responses (e.g. quasi-periodic and chaotic) have been identified. However, the experimental observations along with the analytical/numerical predictions indicate that higher-order nonlinear responses may reside in the transient portion or in the domain of attraction other than quiescent initial conditions. Transitions from one apparent steady-state response to another suggest the presence of an uncontrollable noise component in the wave channel. Stochastic analysis techniques may be needed to further investigate the noise effects on the nonlinear responses.

Acknowledgements—The financial support of the United State Office of Naval Research through Grant No. N00014-92-1221 is gratefully acknowledged. The assistance of Mr Marc A. Myrum and Ms Suchithra Narayanan in data processing and system parameter identification is greatly appreciated.

REFERENCES

Bendat, J. C. and Piersol, A. G. (1993) *Engineering Applications of Correlation and Spectral Analysis*. John Wiley, New York.

Blevins, R. D. (1990) *Flow Induced Vibration*. Van Nostrand Reinhold, New York.

Fujino, M. and Sagara, N. (1990) An analytical of dynamic behaviour of an articulated column in waves. *Journal of the Japan Society of Naval Architects* **4**, 103–112.

Gottlieb, O. and Yim, S. C. S. (1992) Nonlinear oscillations, bifurcations and chaos in a multi-point mooring system with a geometric nonlinearity. *Applied Ocean Research* **14**, 241–257.

Gottlieb, O., Yim, S. C. S. and Lin, H. (1997) Analysis of bifurcation superstructure of a nonlinear ocean system. *Journal of Engineering Mechanics, ASCE*, in press.

Lean, G. H. (1971) Subharmonic motions of moored ships subjected to wave action. RINA 113.

Moon, F. C. (1987) *Chaotic Vibrations*. John Wiley, New York.

Moon, F. C. (1992) *Chaotic and Fractal Dynamics*. John Wiley, New York.

Nayfeh, A. H. and Mook, D. T. (1979) *Nonlinear Oscillations*. John Wiley, New York.

Nayfeh, A. H. and Balachandran, B. (1990) Experimental investigation of resonantly forced oscillations of a two-degree of freedom structure. *International Journal of Nonlinear Mechanics* **25**, 199–209.

Parlitz, U. and Lauterborn, W. (1985) Superstructure in the bifurcation set of the Duffing equation. *Physics Letters* **A107**, 351–355.

Popp, K. and Stelter, P. (1990) Stick–slip vibrations and chaos. *Philosophical Transactions of the Royal Society, London* **A332**, 89–105.

Sarpakaya, T. and Isaacson, M. (1981) *Mechanics of Wave Forces on Offshore Structures*. Van Nostrand Reinhold, New York.

Thompson, J. M. T., Bokaian, A. R. and Ghaffari, R. (1984) Subharmonic and chaotic motions of compliant offshore structures and articulated mooring towers. *Journal of Energy Resource Technology* **106**, 191–198.

Triantafyllou, M. S. and Yue, D. K. P. (1995) Damping amplification in highly extensible hysteretic cables. *Journal of Sound and Vibration* **186**, 355–368.

Yim, S. C. S., Myrum, M. A., Gottlieb, O., Lin, H. and Shih, I.-M. (1993) Summary and Preliminary Analysis of Nonlinear Oscillations in a Submerged Mooring System Experiment. Ocean Engineering Report No. OE-93-03, Oregon State University.